Spectrochimica Acta Part A 82 (2011) 118–125

Contents lists available at ScienceDirect

Spectrochimica Acta Part A: Molecular and Biomolecular Spectroscopy

journal homepage: www.elsevier.com/locate/saa

DFT-based molecular modeling, NBO analysis and vibrational spectroscopic study of 3-(bromoacetyl)coumarin

D. Sajan[a,b], Y. Erdogdu[c,*], R. Reshmy[b], Ö. Dereli[d], K. Kurien Thomas[b], I. Hubert Joe[e]

[a] Department of Physics, Bishop Moore College, Mavelikara, Alappuzha 690110, Kerala, India
[b] Department of Chemistry, Bishop Moore College, Mavelikara, Alappuzha 690110, Kerala, India
[c] Department of Physics, Ahi Evran University, 40040 Kirsehir, Turkey
[d] A. Keleşoğlu Education Faculty, Department of Physics, Selcuk University, Meram 42090, Konya, Turkey
[e] Centre for Molecular and Biophysics Research, Department of Physics, Mar Ivanios College, Thiruvananthapuram 695015, Kerala, India

ARTICLE INFO

Article history:
Received 23 April 2011
Received in revised form 30 June 2011
Accepted 3 July 2011

Keywords:
3-(Bromoacetyl)coumarin
FT-IR and FT-Raman spectra
DFT
NBO

ABSTRACT

The NIR-FT Raman and FT-IR spectra of 3-(bromoacetyl)coumarin (BAC) molecule have been recorded and analyzed. Density functional theory (DFT) calculation of two BAC conformers has been performed to find the optimized structures and computed vibrational wavenumbers of the most stable one. The obtained vibrational wavenumbers and optimized geometric parameters were seen to be in good agreement with the experimental data. Characteristic vibrational bands of the pyrone ring and methylene and carbonyl groups have been identified. The lowering of HOMO–LUMO energy gap clearly explains the charge transfer interactions taking place within the molecule.

1. Introduction

Coumarin is a chemical compound which is found naturally in some plants. Coumarin is found in a variety of plants such as tonka bean, vanilla grass, woodruff, mullein, sweet grass, lavender, sweet clover grass, and licorice, and also occurs in food plants such as strawberries, apricots, cherries, and cinnamon. It is thought to work by serving as a pesticide for the plants that produce it. It can be synthetically produced as well. It has a distinctive odor, which has led people to use it as a food additive and ingredient in perfume. Due to concerns about coumarin as a potential liver and kidney toxin, its use as a food additive is heavily restricted, although it is perfectly safe to eat foods which naturally contain coumarin [1,2].

Coumarins are an important class of compounds because of their applications in synthetic chemistry, medicinal chemistry and photochemistry. Some coumarins are photoactive; they are also widely used in organic solid chemistry [3,4], laser dyes [5,6], biological sensors [7] and molecular switches [8]. Coumarins exhibit antiviral [9] and antimicrobial activities [10]. Coumarins generate strong interest stemming from their great physiological and biological activities, which is further exemplified by their roles as anticoagulants (dicoumarols and its derivatives, warfarin), spasmolytics [11], chemotherapeutics [12], biological inhibitors [13], and [14], antibacterial [15] and antifungal agents [16], bioanalytical reagents [17] or as plant growth regulating agents [18–22]. Coumarin and its derivatives have attracted much interest due to their optical [23] and biological properties [24].

The vibrational spectroscopic techniques (IR and Raman spectroscopy) are powerful molecular structural techniques for the investigation of biological systems. IR and Raman spectroscopy are noninvasive methods yielding molecular fingerprint information; thus, allowing a fast and reliable analysis of complex biological systems such as bacterial or yeast cells.

The IR and Raman spectra serve as a "spectral fingerprint" because it provides comprehensive chemical information for characterization and identification of (cell-) biological systems on a molecular level [25]. Both methods are characterized by a minimal sample preparation and allow for a noninvasive investigation of biological samples. Raman-spectroscopy is especially suited for biological applications because it allows in contrast to IR absorption spectroscopy the analysis of aqueous samples as the Raman signals of water exhibit low Raman intensities [26,27].

Vibrational assignments for the parent coumarin and its derivatives such as dihydro-, 6-methyl and 7-methylcoumarins have been reported based only on spectral correlations [28–31]. IR and Raman spectral investigations of 3-acetylcoumarin [32], 6-methyl-4-bromomethylcoumarin [33] and 7-methyl-4-bromomethyl coumarin [34] supported by *ab initio* density functional theory studies have been reported. Though the crystal structure of the title compound, 3-(bromoacetyl)coumarin (BAC)

---

[*] Corresponding author. Tel.: +90 3862114557; fax: +90 3862114500.
E-mail address: yusuferdogdu@gmail.com (Y. Erdogdu).

1386-1425/$ – see front matter © 2011 Elsevier B.V. All rights reserved.
doi:10.1016/j.saa.2011.07.013

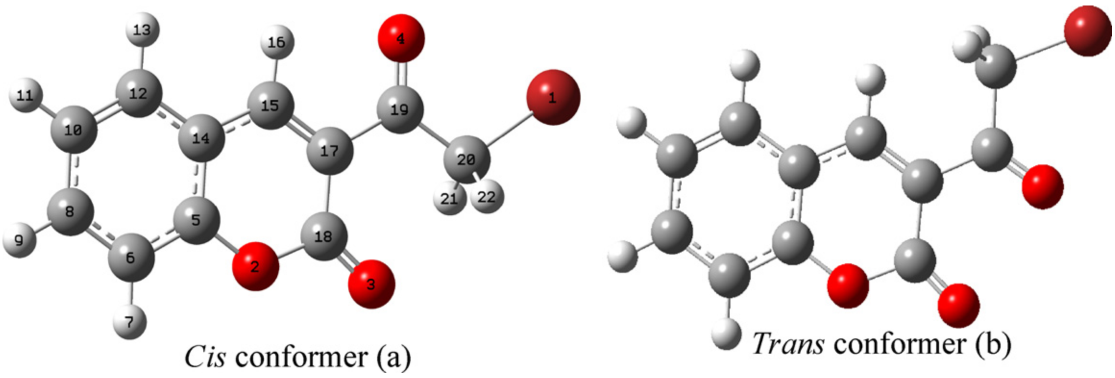

Fig. 1. The conformers and atomic numbering of 3-(bromoacetyl)coumarin.

has been reported [35,36], the vibrational spectral features of BAC crystal have not been subject of detailed analysis so far. The present work describes the vibrational spectral investigations of BAC aided by density functional computations to elucidate the correlation between the molecular structure and biological activity, bonding features, electron delocalization, and the intramolecular charge transfer interactions. Furthermore, we interpreted the calculated spectra in terms of total energy distributions (TEDs) and made the assignment of the experimental bands.

2. Experimental

Salicylaldehyde, ethylacetoacetate, piperidine, glacial acetic acid, ethanol, bromine, and azoisobuteronitrile (AIBN) from Sigma–Aldrich Chemical Company with a stated purity greater than 99% were used without further purification to synthesize the title compound. 3-Bromoacetylcoumarin was synthesized in a two stage process, viz., Knoevenagel condensation and bromination. In the first stage, a mixture of salicylaldehyde (0.01 mmol), ethylacetoacetate (0.01 mmol), piperidine (4 drops), glacial acetic acid (2 drops) and ethanol (20 ml) was refluxed for 5 h and the reaction mixture was poured into cold water, filtered, washed and dried to yield 3-acetylcoumarin. The bromination of 3-acetylcoumarin was carried out using bromine in glacial acetic acid (0.01 mmol) and AIBN as catalyst at about 60–70 °C for 15 min. The crystals of 3-bromoacetylcoumarin formed were collected, washed with minimum quantity of glacial acetic acid, dried and purified by repeated recrystallization from glacial acetic acid to obtain larger size crystals of dimension 28 mm × 7 mm × 3 mm. Purity of the compound was checked by thin layer chromatography. The infrared spectrum of the sample was recorded between 4000 cm^{-1} and 400 cm^{-1} on a JASCO 400 FT-IR spectrometer that was calibrated using polystyrene bands. The sample was prepared as a KBr disc. The FT-Raman spectrum of the sample was recorded the 3500–50 cm^{-1} region on a Bruker RFS 100/S FT-Raman spectrometer using the 1064 nm excitation from a Nd:YAG laser and a liquid nitrogen cooled Ge detector.

3. Computational details

Gaussian 03 quantum chemical software was used in all calculations [37]. The optimized structural parameters and vibrational wavenumbers for the 3-(bromoacetyl)coumarin molecule were calculated by using B3LYP functional with 6-311G(d,p) as basis set. The vibrational modes were assigned on the basis of TED analysis using SQM program [38]. The calculated vibrational wavenumbers were scaled with 0.967 for B3LYP/6-311G(d,p) in order to figure out how the calculated data were in agreement with those of the experimental ones [39].

Table 1
The selected molecular parameters of conformers of BAC for B3LYP/6-311G(d,p) level of theory.

	Cis conformer	*Trans* conformer
Energy (a.u.)	−3223.37231972	−3223.35894185
Relative energy (kcal mol^{-1})	0.000	8.390
E_{HOMO} (eV)	−7.804	−7.804
E_{LUMO} (eV)	−5.873	−5.846
$\Delta E_{\text{HOMO-LUMO}}$ (eV)	−13.677	−13.650
Dipole moment (Debye)	6.627	8.343

4. Results and discussion

4.1. Molecular geometries

The two anticipated stable conformers of BAC are shown in Fig. 1(a) and (b). The energy calculations were carried out for the two possible conformers, namely *cis* and *trans*, of the BAC molecule by B3LYP method at 6-311G(d,p) levels and the results are tabulated in Table 1. The energy obtained for *cis* conformer of BAC molecule at B3LYP was found to be the global minimum.

For BAC molecule, the initial parameters were taken from the work of Sparkes [36] and structure optimizations were performed at the B3LYP levels at 6-311G(d,p) basis set. The optimized bond lengths and bond angles of the *cis* conformer of the BAC molecule at B3LYP level with 6-311G(d,p) as basis set is collected in Table 2. These optimized geometric parameters of BAC are compared with X-ray data of 3-(bromoacetyl)coumarin [36]. The DFT predicted geometric parameters show very good agreement with the experimental data. The averaged CH bond lengths of the coumarin part (C_6H_7, C_8H_9, $C_{10}H_{11}$, $C_{12}H_{13}$, $C_{15}H_{16}$) were determined at 1.085 Å. The $C_{20}H_{21}$ (1.089 Å) and $C_{20}H_{22}$ (1.089 Å) bond lengths for BAC are slightly larger than those of the coumarin part.

4.2. NBO analysis

By the use of the second-order bond–antibond (donor–acceptor) NBO energetic analysis, insight in the most important delocalization schemes was obtained. The change in electron density (ED) in the (σ^*, π^*) antibonding orbitals and $E(2)$ energies have been calculated by natural bond orbital (NBO) analysis [40] using DFT method to give clear evidence of stabilization originating from various molecular interactions. NBO analysis has been performed on BAC in order to elucidate intramolecular hydrogen bonding, intramolecular charge transfer (ICT) interactions and delocalization of π-electrons of the coumarin ring. The hyperconjugative inter-

Table 2
Optimized geometric parameters of *cis* conformer of BAC for B3LYP calculations.

Bond lengths (Å)	6-311G(d,p)	X-ray [36]	Bond angles (°)	6-311G(d,p)	X-ray [36]
$Br_1–C_{20}$	1.957	1.934	$C_5–O_2–C_{18}$	123.6	122.9
$O_2–C_5$	1.359	1.368	$O_2–C_5–C_6$	117.8	117.3
$O_2–C_{18}$	1.396	1.383	$O_2–C_5–C_{14}$	120.8	121.1
$O_3–C_{18}$	1.202	1.201	$C_6–C_5–C_{14}$	121.2	121.5
$O_4–C_{19}$	1.209	1.214	$C_5–C_6–H_7$	119.1	120.6
$C_5–C_6$	1.393	1.389	$C_5–C_6–C_8$	118.7	118.7
$C_5–C_{14}$	1.405	1.394	$H_7–C_6–C_8$	122.0	120.6
$C_6–H_7$	1.082	0.950	$C_6–C_8–H_9$	119.2	119.5
$C_6–C_8$	1.387	1.382	$C_6–C_8–C_{10}$	121.0	120.9
$C_8–H_9$	1.083	0.950	$H_9–C_8–C_{10}$	119.6	119.5
$C_8–C_{10}$	1.403	1.407	$C_8–C_{10}–H_{11}$	119.9	120.2
$C_{10}–H_{11}$	1.082	0.950	$C_8–C_{10}–C_{12}$	119.8	119.6
$C_{10}–C_{12}$	1.382	1.380	$H_{11}–C_{10}–C_{12}$	120.2	120.2
$C_{12}–H_{13}$	1.084	0.950	$C_{10}–C_{12}–H_{13}$	120.8	119.8
$C_{12}–C_{14}$	1.408	1.403	$C_{10}–C_{12}–C_{14}$	120.3	120.3
$C_{14}–C_{15}$	1.427	1.429	$H_{13}–C_{12}–C_{14}$	118.8	119.8
$C_{15}–H_{16}$	1.085	0.950	$C_5–C_{14}–C_{12}$	118.7	118.8
$C_{15}–C_{17}$	1.361	1.355	$C_5–C_{14}–C_{15}$	117.3	117.3
$C_{17}–C_{18}$	1.465	1.463	$C_{12}–C_{14}–C_{15}$	123.9	123.8
$C_{17}–C_{19}$	1.510	1.502	$C_{14}–C_{15}–H_{16}$	120.1	119.0
$C_{19}–C_{20}$	1.521	1.507	$C_{14}–C_{15}–C_{17}$	122.1	121.9
$C_{20}–H_{21}$	1.088	0.990	$H_{16}–C_{15}–C_{17}$	117.7	119.0
$C_{20}–H_{22}$	1.088	0.990	$C_{15}–C_{17}–C_{18}$	119.9	119.9
			$C_{15}–C_{17}–C_{19}$	117.3	117.5
			$C_{18}–C_{17}–C_{19}$	122.7	122.5
			$O_2–C_{18}–O_3$	116.7	115.9
			$O_2–C_{18}–C_{17}$	116.0	116.6
			$O_3–C_{18}–C_{17}$	127.2	127.4
			$O_4–C_{19}–C_{17}$	119.2	119.1
			$O_4–C_{19}–C_{20}$	122.8	122.2
			$C_{17}–C_{19}–C_{20}$	117.8	118.5
			$Br_1–C_{20}–C_{19}$	112.9	112.4
			$Br_1–C_{20}–H_{21}$	107.6	109.1
			$Br_1–C_{20}–H_{22}$	107.6	109.1
			$C_{19}–C_{20}–H_{21}$	110.7	109.1
			$C_{19}–C_{20}–H_{22}$	110.7	109.1
			$H_{21}–C_{20}–H_{22}$	106.9	107.8

action energy was deduced from the second-order perturbation approach [41].

$$E(2) = -n_\sigma \frac{\langle \sigma | F | \sigma \rangle^2}{\varepsilon_{\sigma^*} - \varepsilon_\sigma} = -n_\sigma \frac{{F_{ij}}^2}{\Delta E}, \qquad (1)$$

where $\langle \sigma | F | \sigma \rangle^2$ or F_{ij}^2 is the Fock matrix element between the i and j NBOs, ε_σ and ε_{σ^*} are the energies of σ and σ^* NBOs, and n_σ is the population of the donor σ orbital.

The most important interactions between Lewis and non-Lewis orbitals with O lone pairs are the second order perturbation energy values, $E(2)$, corresponding to these interactions, and the overlap integral of each orbital pair. A very strong interaction has been observed between the p-type orbital containing the lone electron pair of O_2 and the neighbor $\pi^*(C_{14}–C_5)$, $\pi^*(C_{18}–O_3)$ antibonding orbital of the benzene ring. The p electrons of C_{14} and C_{18} toward the $n(\text{LP2 } O_2)$ orbital and the overlap of the donor and acceptor orbitals are notorious. The energy contribution of (LP2 O_4) → σ^* ($C_{17}–C_{19}$), (LP2 O_2) → σ^* ($C_3–O_3$) and (LP2 O_2) → σ^* ($C_5–C_{14}$) values are 21.12 kcal mol^{-1}, 36.98 kcal mol^{-1} and 31.60 kcal mol^{-1}, respectively. This interaction is responsible for a pronounced decrease of the lone pair orbital occupancy 1.98278 than the other occupancy, and there is a possibility for hyperconjugation between O_2 and the benzene ring. An important contribution for the molecular stabilization is further given by O_3 through the overlap of its sp 1.38 lone pair $n(\text{LP1 } O_3)$ with the $\sigma^*(C_{18}–C_{17})$ orbital. The energy contribution of LP2 $O_3 \rightarrow \sigma^*$ ($C_{18}–O_2$) value is 38.22 kcal mol^{-1}.

4.3. *Vibrational analysis*

The *cis* conformer of 3-(bromoacetyl)coumarin (Fig. 1) molecule belongs to C_s symmetry. BAC molecule consists of 22 atoms, which has 60 normal modes. The 60 normal vibrations are distributed as 40A′ (in-plane) + 20A″ (out-of-plane). All the vibrations are active in both IR and Raman spectra. The calculated frequencies together with the experimental data of BAC molecule are presented in Table 3. Theoretical and experimental (IR and Raman) spectra of BAC are given in Figs. 2 and 3. The total energy distribution (TED) was calculated by using the SQM program [38] and the fundamental vibrational modes were characterized by their TED.

The Raman activities (S_i) calculated with Gaussian 03 program converted to relative Raman intensities (I_i) using the following relationship derived from the intensity theory of Raman scattering [42,43]:

$$I_i = \frac{f(\nu_0 - \nu_i)^4 S_i}{\nu_i[1 - \exp(-((hc\nu_i)/(kT)))]}, \qquad (2)$$

with ν_0 being the exciting wavenumber in cm^{-1}, ν_i the vibrational wavenumber of ith normal mode, h, c and k universal constants and f is a suitably chosen common normalization factor for all peak intensities. For visual comparison, the observed and simulated FT-IR and FT-Raman spectra are presented in Figs. 2 and 3, respectively.

4.3.1. *C–H vibrations*

The aromatic structure shows the presence of the C–H stretching vibrations in the region 3100–3000 cm^{-1} which is the characteristic region for the identification of the C–H stretching vibrations [47–49]. The C–H vibrations of the 3-acetylcoumarin

Table 3
Observed and calculated vibrational modes of *cis* conformer of BAC (cm^{-1}).

Mode no.	Symmetry	Theoretical B3LYP/6-311G(d,p)			Experimental		TED (%)[d]
		Scaled freq[a]	I_{IR}[b]	I_{Raman}[c]	Exp. IR	Exp. Raman	
ν_{60}	A'	3104	0.5	4.6	3109 w		$\nu_{CH}(99)$
ν_{59}	A'	3093	1.8	4.3	3083 vw		$\nu_{CH}(100)$
ν_{58}	A'	3078	0.7	2.9	3088 vw		$\nu_{CH}(99)$
ν_{57}	A'	3074	0.3	1.0	3067 w	3067 s	$\nu_{CH}(98)$
ν_{56}	A'	3071	0.0	0.6	3046 m	3026 s	$\nu_{CH}(98)$
ν_{55}	A''	3053	0.1	0.8		2994 vw	$\nu_{CH}(100)$ CH_2
ν_{54}	A'	3005	2.9	2.5	2960 s	2959 m	$\nu_{CH}(100)$ CH_2
ν_{53}	A'	1747	13	7.3	1746 w		$\nu_{CO}(85)$
ν_{52}	A'	1713	100	6.4	1731 vs	1719 m	$\nu_{CO}(86)$
ν_{51}	A'	1596	27	76	1603 s	1607 s	8a $\nu_{CC}(67)$
ν_{50}	A'	1582	11	20	1577 vw	1599 s	8b$\nu_{CC}(63)$
ν_{49}	A'	1537	39	100	1556 vs	1559 vs	19a $\nu_{CC}(66)+\beta_{CCH}(11)$
ν_{48}	A'	1467	1.6	9.2	1486 m	1489 w	$\nu_{CC}(37)+\beta_{CCH}(41)$
ν_{47}	A'	1431	6.4	14	1449 s	1453 m	19b $\nu_{CC}(34)+\beta_{CCH}(45)$
ν_{46}	A'	1374	2.9	2.7	1370 m	1362 w	$\delta_{CH_2}(56)$
ν_{45}	A'	1345	2.2	0.8		1335 m	$\nu_{CC}(35)+\beta_{CCH}(36)$
ν_{44}	A'	1324	0.0	44	1301 m	1304 vw	14$\nu_{CC}(84)$
ν_{43}	A'	1275	1.3	3.8	1269 vw	1271 w	$\nu_{CC}(20)+\omega_{CCH}(29)$
ν_{42}	A'	1245	2.3	7.7	1226 vw		$\nu_{CC}(14)+\beta_{CCH}(35)+\omega_{HCBr}(15)$
ν_{41}	A'	1233	4.0	0.4	1216 vw	1216 s	$\nu_{CO}(11)+\nu_{CC}(17)+\omega_{CCH}(23)$
ν_{40}	A'	1203	0.6	40	1205 vw		$\nu_{CO}(22)+\nu_{CC}(28)+\beta_{CCH}(26)$
ν_{39}	A'	1145	15	6.4	1153 m	1148 vw	$\nu_{CC}(12)+\tau_{CCH}(62)$
ν_{38}	A'	1124	31	1.9	1126 w	1123 vw	$\nu_{CC}(31)+\beta_{CCH}(28)$
ν_{37}	A''	1124	0.2	3.9			$\beta_{HCBr}(32)+\tau_{CCH}(57)$
ν_{36}	A'	1105	5.3	1.1	1053 m	1059 s	$\nu_{CC}(27)+\beta_{CCH}(47)$
ν_{35}	A'	1013	0.2	34	1030 vw	1028 m	$\nu_{CC}(60)+\beta_{CCH}(24)$
ν_{34}	A'	1009	3.6	17	992 w		$\nu_{CC}(37)+\beta_{OCC}(13)$
ν_{33}	A''	980	1.2	1.2	983 m	982 m	$\gamma_{CCH}(40)+T_{CCCC}(38)$
ν_{32}	A''	968	0.1	0.0			$\gamma_{CCH}(66)+T_{CCCH}(10)$
ν_{31}	A''	935	0.1	0.0			$\gamma_{CCH}(43)+T_{CCCH}(34)$
ν_{30}	A'	928	14	15	919 s		$\nu_{CO}(53)+\nu_{CC}(19)$
ν_{29}	A'	904	1.2	2.9			$\delta_{CCC}(43)+\beta_{CCH}(12)$
ν_{28}	A''	855	1.0	0.8	876 m		$\rho_{CH_2}(10)(13)+\gamma_{CCH}(33)+T_{OCCBr}(10)$
ν_{27}	A''	849	2.6	0.3		830 w	$T_{OCCH}(11)+\gamma_{CCH}(40)\ \rho_{CH_2}(10)$
ν_{26}	A'	808	0.1	13			$\nu_{CC}(61)+\beta_{CCC}(10)$
ν_{25}	A''	754	12	1.8	755 s		$T_{OCCC}(36)+\gamma_{CCC}(12)\ \rho_{CH_2}(10)$
ν_{24}	A''	747	0.0	1.5	734 vw	739 s	$\gamma_{CCH}(65)$
ν_{23}	A'	732	0.9	4.5			$\nu_{CC}(18)+\beta_{CCC}(33)+\beta_{OCC}(12)$
ν_{22}	A'	721	0.0	65			$\nu_{CC}(32)+\beta_{OCC}(21)$
ν_{21}	A''	720	0.3	0.7			$T_{CCCC}(40)+\gamma_{CCH}(21)+T_{CCCO}(11)$
ν_{20}	A'	646	10	43	670 s	672 s	$\nu_{CC}(10)+\nu_{CBr}(34)+\beta_{CCC}(14)$
ν_{19}	A'	623	0.2	21	633 w	635 w	$\beta_{CCO}(14)+\beta_{OCO}(10)+\beta_{CCC}(25)$
ν_{18}	A'	560	2.2	8.4	573 m	568 vw	$\beta_{CCO}(19)+\beta_{CCC}(22)$
ν_{17}	A'	542	10	21	553 s	552 w	$\nu_{CBr}(16)+\beta_{CCC}(16)+\beta_{CCO}(27)$
ν_{16}	A''	542	0.0	0.7			$\rho_{CH_2}(10)+T_{CCCC}(42)+\gamma_{CCH}(16)$
ν_{15}	A''	530	0.1	1.0			$\rho_{CH_2}(15)+T_{OCCC}(21)+\gamma_{CCH}(27)$
ν_{14}	A''	454	0.8	1.8	452 w	454 m	$T_{CCCC}(36)+\gamma_{CCH}(17)$
ν_{13}	A'	442	0.1	70	410 vw		$\nu_{CO}(14)+\nu_{CC}(11)+\beta_{CCC}(28)+\beta_{CCO}(11)$
ν_{12}	A''	373	0.0	21		377 w	$\gamma_{CCH}(15)+T_{CCCC}(46)+\rho_{CH_2}(10)$
ν_{11}	A'	366	0.6	9.2			$\nu_{CC}(19)+\beta_{OCC}(24)+\beta_{CCC}(18)$
ν_{10}	A'	319	0.8	18		328 vw	$\beta_{CCH}(32)+\beta_{CCO}(34)$
ν_{9}	A''	270	0.2	0.0			$T_{CCCO}(27)+T_{CCCC}(28)$
ν_{8}	A'	228	0.4	0.3		238 w	$\beta_{CCC}(44)+\beta_{CCBr}(13)+\beta_{CCO}(13)$
ν_{7}	A''	221	0.2	0.2			$\gamma_{CCC}(28)+T_{CCCO}(27)+\rho_{CH_2}(13)$
ν_{6}	A'	168	0.4	0.7		182 m	$\nu_{CC}(21)+\nu_{CBr}(24)+\beta_{CCBr}(20)$
ν_{5}	A''	101	0.3	0.4		120 s	$\gamma_{OCCC}(19)+T_{CCCC}(25)+T_{CCOC}(25)$
ν_{4}	A''	94	0.9	1.6			$T_{OCCBr}(18)+\rho_{CH_2}(16)+\tau_{CCCH}(13)$
ν_{3}	A'	94	0.3	0.7			$\beta_{OCC}(10)+\beta_{CCC}(51)+\beta_{CCBr}(21)$
ν_{2}	A''	61	0.4	0.9			$\gamma_{OCC}(54)+\rho_{CH_2}(14)$
ν_{1}	A''	20	0.3	6.9			$T_{CCCBr}(20)+\gamma_{OCC}(39)+T_{CCCH}(15)$

ν: stretching, ρ: rocking, ω: wagging, γ: out-of-plane bending, β: in-plane bending, δ: scissoring, τ: twisting, T: torsion, vw: very week, w: week, m: medium, s: strong, vs: very strong.

[a] Scaling factor: 0.967.

[b] Relative absorption intensities normalized with highest peak absorption equal to 100.

[c] Relative Raman intensities calculated by Eq. (2) and normalized to 100.

[d] Total energy distribution calculated B3LYP/6-311G(d,p) level, TED less than 10% is not shown.

are observed at 3079, 3068, 3046 and 3029 cm^{-1} in the FT-IR spectrum and at 3081, 3070, 3047 and 3029 cm^{-1} in the FT-Raman [34,50]. The observed bands in IR at 3067, 3088 and 3109 cm^{-1} attributed to C–H stretching vibrations of coumarin part. DFT computations predict these modes at 3074, 3078 and 3104 cm^{-1} for B3LYP/6-311G(d,p) level of theory. The results showed that the experimental and theoretical data were in good agreement.

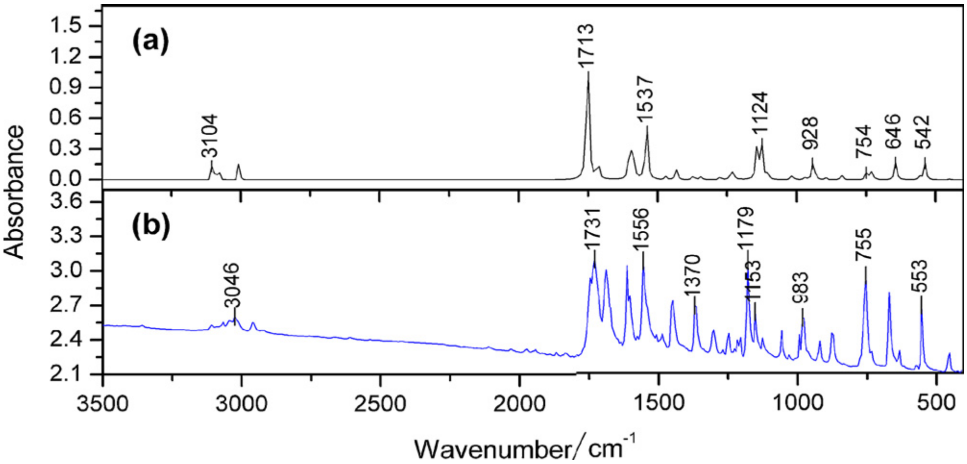

Fig. 2. Theoretical (B3LYP with 6-311G(d,p) (a)) and experimental (b) (powder form) infrared spectra of 3-(bromoacetyl)coumarin.

The C–H stretching modes of acetyl group in the 3-acetylcoumarin were observed at 2984, 2959 and 2931 cm^{-1} in the FT-IR spectra [33,51]. The CH stretching vibrations of the acetyl group were determined lower than those of the coumarin part. The antisymmetric stretching ($\nu_{as}CH_2$) and symmetrical stretching ($\nu_{s}CH_2$) bands of methylene groups occur near 2926 and 2853 cm^{-1}, respectively [47–49]. The qualitative interpretation of intensities must rely upon the understanding of some basic aspects of intramolecular charge distribution and on their effects on infrared intensities. The methylene group hydrogen atoms in BAC are subjected to the electronic effect of hyperconjugation leading to the decrease of infrared intensities and blue shifting of stretching wavenumbers, as discussed in the preceding methyl vibrations section. The methylene antisymmetric stretching manifests its characteristic band at 2994 cm^{-1} in Raman as weak band and DFT computations predict this mode at 3053 cm^{-1}. The symmetric stretching vibration is observed at 2960 cm^{-1} in IR spectrum and at 2959 cm^{-1} in Raman. The changes in intensity of the CH_2 stretching mode in infrared spectrum and shift the wavenumber to the higher wavenumbers owing to the proximity of the high electronegative bromine atom resulting from hyperconjugation of the methylene group with the aromatic ring system [52].

The four bending vibrations of C–H bonds in the methylene groups are referred to as scissoring, twisting, wagging and rocking and they are identified. The (δ_s CH_2) scissoring vibrations are expected in the region 1455–1380 cm^{-1} and consist of medium intense bands [47–49]. This scissoring mode is characterized by the IR band at 1370 cm^{-1} and Raman at 1362 cm^{-1}, which is computed at 1374 cm^{-1}. In BAC the wagging vibrations of CH_2 are found in both IR and Raman spectrum near 1270 cm^{-1} which is justified by our DFT calculation also. The twisting and rocking vibrations of CH_2 group are observed at 1148 cm^{-1} and 830 cm^{-1} in Raman spectrum respectively which is supported by results reported in literature [47–49].

The in plane C–H bending of aromatic compounds vibrations [47–49] appears in the region 1400–1050 cm^{-1}. The C–H in plane bending vibrations may be identified in BAC at 1335, 1148 and 1059 cm^{-1} in Raman spectrum are also supported by computed results. These modes are observed in the IR spectrum also in the same region. The absorption bands arising from C–H out of plane bending vibrations [47–49] are usually observed in the region from 1000 cm^{-1} to 675 cm^{-1}. The out of plane bending vibrations in BAC are observed as medium bands at 982 cm^{-1}, 830 cm^{-1} and 739 cm^{-1} in Raman spectrum and the corresponding IR bands are at 983 cm^{-1} and 734 cm^{-1}, respectively. Bromine compounds [48] show stretching vibrations in the region 750–485 cm^{-1} due to C–Br. In the present case, the band at 670 cm^{-1} in IR and 672 cm^{-1} in Raman is assigned as the C-Br stretching mode. The C-Br deformations [49] are found in the region 400–140 cm^{-1}. The observed bands in Raman at 182 cm^{-1} and 238 cm^{-1} are assigned to C-Br deformation mode.

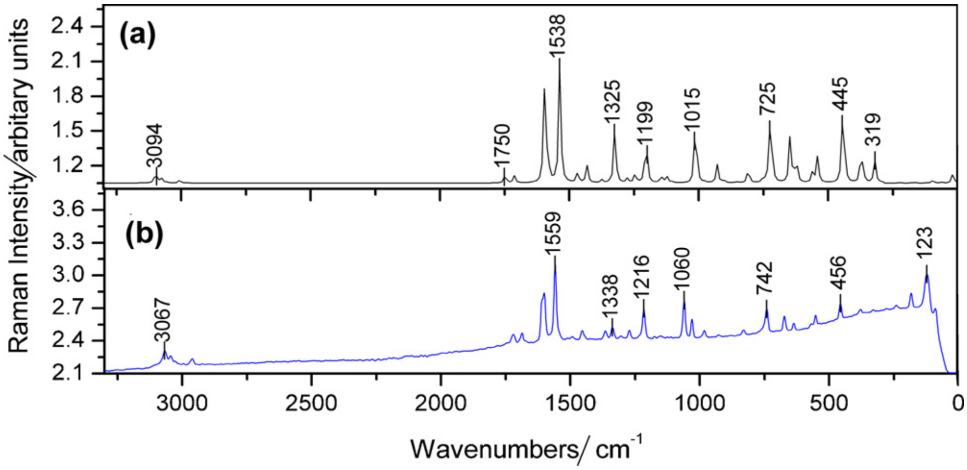

Fig. 3. Theoretical (B3LYP with 6-311G(d,p) (a)) and experimental (b) (powder form) Raman spectra of 3-(bromoacetyl)coumarin.

4.3.2. Carbonyl vibrations

The acetyl carbonyl group bonded to the pyrone ring gives rise to a series of characteristic bands corresponding to the carbonyl and methylene moieties. The intensity of these bands can increase because of conjugation or formation of hydrogen bonds. The increase of conjugation, therefore, leads to the intensification of the Raman lines as well as increased infrared band intensities. The carbonyl stretching wavenumber of the 3-acetylcoumarin is observed sharp intense bands in IR spectrum at 1684 cm^{-1}, which is also observed in Raman at 1675 cm^{-1} as medium intensity bands [34,50]. The sharp intense band in infrared spectrum at 1731 cm^{-1} is assigned to $C_{19}{=}O_4$ stretching mode, which is also observed in the Raman spectrum at 1719 cm^{-1} as a medium intense band. The results of computations give the wavenumber of this mode as 1713 cm^{-1}. It is evident that the $C_{19}{=}O_4$ stretching mode is blue shifted by 25 cm^{-1} compared to 3-acetylcoumarin. This means that in the acetyl part C=O vibration is sensitive to the proximity of the high electronegative bromine atom. The blue shifting of C=O stretching wavenumber is further influenced by the hyperconjugation with the C_{18}–C_{17} bond, which is confirmed by NBO analysis.

The carbonyl bands are most characteristic bands of the IR and Raman spectrum [44–46]. The carbonyl stretching vibrations are found in the region 1780–1700 cm^{-1} [47–49]. A weak IR absorption band at 1746 cm^{-1} corresponds to the carbonyl vibration in the pyrone ring [32–34,50]; the corresponding theoretical band with the comparable intensity at 1747 cm^{-1}. The $C_{18}{=}O_3$ bond has in the alpha position atom O_2 and belongs to the ester group, therefore its wavenumber is higher than the wavenumber of the ketone carbonyl group $C_{19}{=}O_4$. In BAC, the C=O bond in the lactone part is conjugated with $C_{15}{=}C_{17}$ and $C_{14}{=}C_5$ double bonds. In the present study, the carbonyl vibrational wavenumbers in the lactone part $C_{18}{=}O_3$ stretching have been lowered to different extents due to conjugation, which is supported by NBO results also. The C_{18}–O_2 and C_5–O_2 stretching bands are observed at 1216 and 919 cm^{-1}, respectively, in IR spectrum as medium intensity bands whereas the corresponding Raman bands are observed at nearby positions, at 1216 cm^{-1}, respectively. The C–O skeletal mode is less stable and sensitive; it may be assigned to a weak Raman band at 971 cm^{-1}.

4.3.3. Ring vibrations

The C–C ring stretching vibrations have given rise to characteristic bands in both the observed IR and Raman spectra, covering the spectral range from 1610 to 1300 cm^{-1} [32–34,47–49]. The observed bands at 1617, 1603, 1556, 1338, 1109, 807 and 748 cm^{-1} in both infrared and Raman spectra for acetyl coumarin have been attributed to the ring stretching vibrations [34,50]. In BAC, the ring mode manifests as strong bands in Raman spectrum at 1607 cm^{-1} and 1599 cm^{-1}. The observed bands at 1603 cm^{-1} and 1577 cm^{-1} in IR correspond to ring mode, which are localized on the benzene part of the molecule. These vibrations correspond to the e_g mode (8a) of benzene [51] at 1610 cm^{-1}. The band at 1559 cm^{-1}, 1489 and 1453 cm^{-1} in infrared spectrum contain C–C stretching and aromatic C–H in plane bending character as well as minor contributions from other modes [47–49]. These modes are observed in the Raman spectrum also in the same region. Both modes are mainly vibrations of the benzene ring and correspond to the e_{1u} mode of benzene at 1484 cm^{-1}, which is calculated to be 1476 cm^{-1}. The intense band respectively for both in infrared and Raman spectrum at 1301 cm^{-1} and 1304 cm^{-1} is predominantly a C–C stretching of benzene, which is justified by PED results also. The infrared bands identified at 633 cm^{-1} and 573 cm^{-1}, for BAC have been designated to ring in-plane bending modes, by careful consideration of their quantitative descriptions. Small changes in wavenumber observed for these modes are due to the changes in force constant/reduced mass ratio, resulting mainly due to addition of bromoacetyl group to coumarin and from different extents of mixing between ring and substituent group vibrations. The ring in-plane, and out-of-plane bending vibrations have been identified and presented in Table 3. They are also supported by the literature [47–49]. The simultaneous IR and Raman activation of the ring mode and carbonyl mode clearly explains the charge transfer interaction between the electron-donating group and the acceptor group through the π-conjugated system. The π-electron cloud movement from the donor to the acceptor can make the molecule highly polarized through the single/double path, when it changes from the ground state into the first excited state [52–54]. It is inferred that this mechanism plays an important role in the biological activity of BAC.

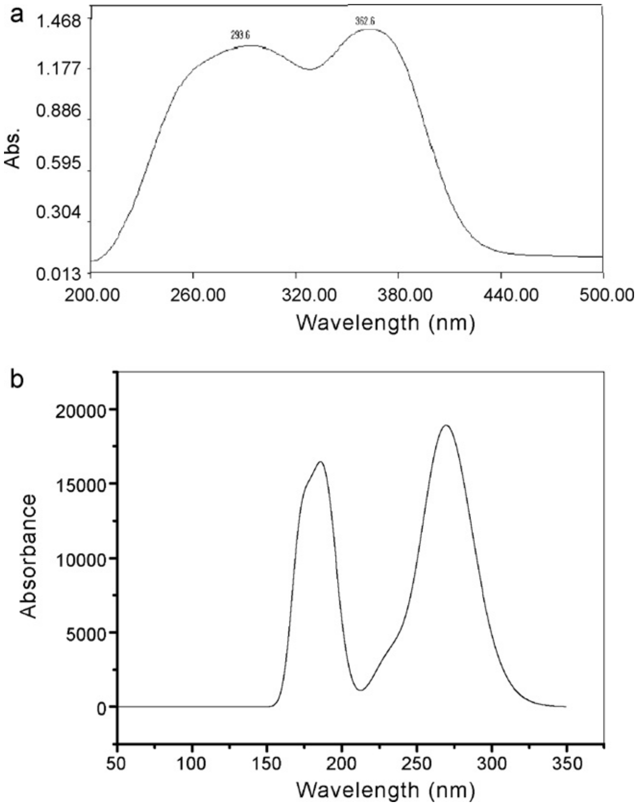

Fig. 4. Experimental UV spectrum of BAC (a) and TD-DFT//B3LYP/6-311G(d,p) level UV spectrum of BAC (b).

4.4. Electronic spectra

The chemical structure of BAC is composed of a conjugated system of double bonds and aromatic ring. Natural bond orbital analysis indicates that molecular orbitals are mainly composed of π atomic orbital, so above electronic transitions are mainly derived from the contribution of bands π–π^*. UV–vis absorption spectrum of the sample in Methanol is shown in Fig. 4. The strong transitions with λ_{max} at 363 and 293 nm have been observed are assigned to a π–π^* transition. The π–π^* transitions with λ_{max} at 324 nm is mainly localized in the pyrone ring [55]. The TD-DFT is particularly well suited to low energy valence excited states that can be described by combinations of single excitations. These are identified with the calculated transitions at 270 and 188 nm. In this case, the first energy transition is blue shifted from the experimental value by 90 nm because the theoretical spectrum was obtained in gas phase without considering the solvent effect of the molecule. This electronic absorption corresponds to the transition from the ground to the first excited state and is mainly described by one electron excitation from the highest occupied molecular orbital (HOMO) to the lowest unoccupied molecular orbital (LUMO).

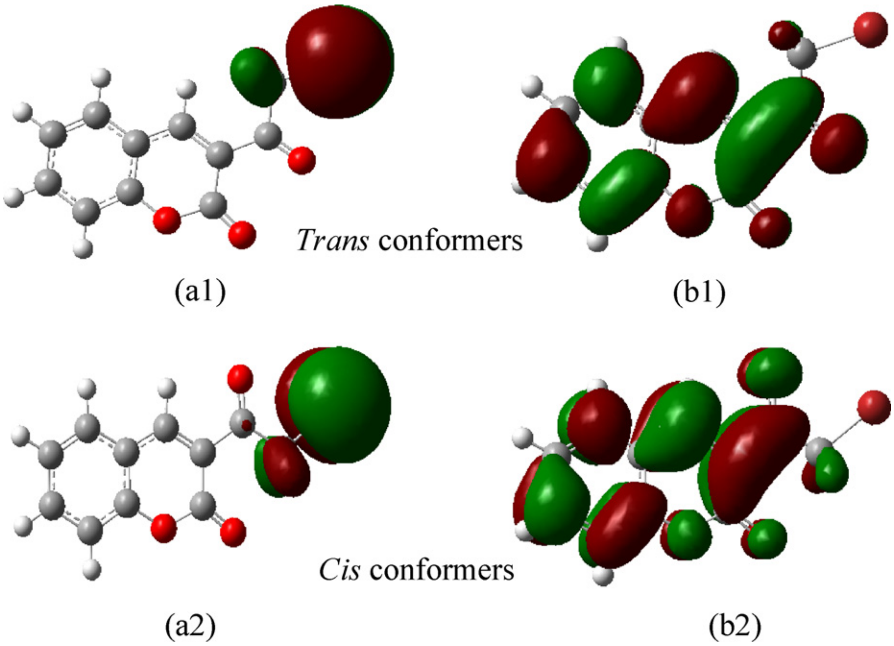

Fig. 5. HOMO (a1, a2) and LUMO (b1, b2) plots of *cis* and *trans* conformers.

4.5. HOMO, LUMO analysis

The conjugated molecules are characterized by a small highest occupied molecular orbital–lowest unoccupied molecular orbital (HOMO–LUMO) separation, which is the result of a significant degree of intramolecular charge transfer (ICT) from the end-capping electron-donor groups to the efficient electron-acceptor groups through π-conjugated path. The strong charge transfer interaction through π-conjugated bridge results in substantial ground state donor–acceptor mixing and the appearance of a charge transfer band in the electronic absorption spectrum. Consequently, an ED transfer occurs from the more aromatic part of the π-conjugated system in the electron donor side to its electron-withdrawing part mainly of quinonoid form. Furthermore, the HOMO and LUMO topologies show certain overlap of two orbitals in the middle region of the π-conjugated systems, which is a prerequisite to allow an efficient charge transfer transition [52–54]. The HOMO is located over acetyl carbonyl group, and the HOMO → LUMO transition implies an electron density transfer to the bromoacetyl group from the coumarin ring. The atomic orbital compositions of the frontier molecular orbitals of *cis* and *trans* conformers of BAC are sketched in Fig. 5. The HOMO–LUMO energy gap of BAC was calculated at the B3LYP/6-311G(d,p) level, which reveals that the energy gap reflects the chemical activity of the molecule. The LUMO as an electron acceptor represents the ability to obtain an electron, and HOMO represents the ability to donate an electron. The energy gap (−13.677 eV) of HOMO–LUMO explains the eventual charge transfer interaction within the molecule, which influences the biological activity of the molecule. Consequently, the lowering of the HOMO–LUMO band gap is essentially a consequence of the large stabilization of the LUMO due to the strong electron-acceptor ability of the electron-acceptor group.

5. Conclusion

FT-IR and FT-Raman spectra of the 3-(bromoacetyl)coumarin (BAC) have been recorded and analyzed. Density functional theory (DFT) calculations at the B3LYP/6-311G(d,p) level has been used to compute energies of different conformers of BAC to find out their stability, the optimized geometry of the most stable conformer and its vibrational spectrum. The energy calculations were carried out for the two possible conformers namely *cis* and *trans* of the BAC molecule. The energy obtained for *cis* conformer of BAC molecule at B3LYP was found to be the global minimum. The vibrational modes were assigned on the basis of TED analysis and analyzed by using SQM program. The observed vibrational wavenumbers and optimized geometric parameters were seen to be in good agreement with the experimental data. The intramolecular charge transfers (ICT), π-electron delocalization and its related processes have been comprehensively investigated for the prospective BAC from vibrational spectroscopy and DFT computations. The lowering of HOMO–LUMO energy gap clearly explains the charge transfer interactions taking place within the molecule. It is possible to understand intramolecular charge transfer mechanisms between the groups by comparing the charges on atoms.

Acknowledgements

We thank referees for their valuable suggestions. The author (Y. Erdogdu) would like to thank Ahi Evran University Research Fund for its financial support, Project Numbers: A10/2009. We also thank Assoc. Prof. Dr. Mustafa Kurt for the Gaussian 03W program package.

References

[1] http://micro.magnet.fsu.edu/phytochemicals/pages/coumarin.html.
[2] http://en.wikipedia.org/wiki/Coumarin.
[3] J.T. Brett, J. Alexander, M.J.J. Stezowski, J. Chem. Soc. Perkin Trans. 2 (2000) 1095–1103.
[4] K. Vishnumurthy, T.N. Guru Row, K. Venkatesan, Photochemistry (2001) 427–460.
[5] N.A. Nemkovich, H. Reis, W. Baumann, J. Lumin. 71 (1997) 255–263.
[6] V.K. Sharma, P.D. Saharo, N. Sharma, R.C. Rastogi, Spectrochim. Acta A 59 (2003) 1161–1170.
[7] S. Sardari, Y. Mori, K. Horita, R.G. Micetich, S. Nishibe, M. Daneshtalab, Bioorg. Med. Chem. 7 (1999) 1933–1940.
[8] M.B. Maria, Z.Y. Wang, Tetrahedron Lett. 41 (2000) 4025–4028.
[9] J.M. Domagala, S.E. Hagen, E.T. Lunney, D. Bradly, Warner-Lambert Co. USA, US Patent No. 5 (1996) 5103 75.
[10] A.I. Eid, F.A. Ragab, S.L. El-Ansary, S.M. El-Gazayerly, F.E. Mourad, Arch. Pharm. 327 (1994) 211–213.
[11] J.W. Suttie, Clin. Cardiol. 13 (1990) 16.

[12] D.A. Egan, P. James, D. Cooke, R. O'Kennedy, Cancer Lett. 118 (1997) 201.
[13] C. Gnerre, M. Catto, F. Leonetti, P. Weber, P.A. Carrupt, C. Altomare, A. Carotti, B.J. Testa, J. Med. Chem. 43 (2000) 4747.
[14] F. Chimenti, D. Secci, A. Bolasco, P. Chimenti, A. Granese, O. Befani, P. Turini, S. Alcaro, F. Ortuso, Bioorg. Med. Chem. Lett. 14 (2004) 3697.
[15] A.H. Bedair, N.A. El-Hady, M.S. Abd El-Latif, A.H. Fakery, A.M. El-Agrody, Farmaco 55 (2000) 708.
[16] T. Patonay, G. Litkei, R. Bognar, J. Eredi, C. Miszti, Pharmazie 39 (1984) 86–91.
[17] M. Jiménez, J.J. Mateo, J. Chromatogr. A 870 (2000) 473.
[18] U.P. Masche, K.M. Rentsch, A. Felten, P.J. Meier, K.E. Fittinger, Eur. J. Clin. Pharmacol. 54 (1999) 865.
[19] J. Parrish, T. Fitzpatrick, L. Tannenbaum, M. Patak, N. Engl. J. Med. 291 (1974) 1207.
[20] G. Luzzatto, F. Fabris, R. Dal Bo Zanon, A. Giralami, Arzneim.-Forsch. 36 (1986) 972.
[21] I.P. Kostova, I. Manolov, I. Nicolova, N. Danchev, Farmaco 56 (2001) 707.
[22] A. Gursoy, N. Karali, Turk. J. Chem. 27 (2003) 545.
[23] X. Yu, D. Scheller, O. Rademacher, T. Wolff, J. Org. Chem. 68 (2003) 7386–7399.
[24] C. Gnerre, M. Catto, F. Leonetti, P. Weber, P.A. Carrupt, C. Altomare, B. Testa, J. Med. Chem. 43 (2000) 4747–4758.
[25] K. Maquelin, L.-P. Choo-Smith, C. Kirschner, T.N.A. Ngo, D. Naumann, G.J. Puppels, Vibrational spectroscopic studies of microorganisms, in: J.M. Chalmers, P.R. Griffiths (Eds.), Handbook of Vibrational Spectroscopy, John Wiley, Chichester, 2002.
[26] R. Petry, M. Schmitt, J. Popp, J. Raman Spectrosc. 4 (2003) 14–30.
[27] E. Urlaub, J. Popp, W. Kiefer, G. Bringmann, D. Koppler, H. Schneider, U. Zimmermann, B. Schrader, Biospectroscopy 4 (1998) 113–120.
[28] R.S. Rasmussen, R.R. Brattain, J. Am. Chem. Soc. 71 (1949) 1073.
[29] C.P. Girijavallabhan, K. Venkateswarlu, Curr. Sci. 37 (1968) 11.
[30] S.S. Saleem, G. Aruldhas, Indian J. Pure Appl. Phys. 21 (1984) 110.
[31] S.R. Tripati, N.K. Sanyal, Ind. J. Phys. 63B (1989) 474.
[32] V. Sortur, J. Yenagi, J. Tonannavar, V.B. Jadhav, M.V. Kulkarni, Spectrochim. Acta A 64 (2006) 301.
[33] V. Sortur, J. Yenagi, J. Tonannavar, V.B. Jadhav, M.V. Kulkarni, Spectrochim. Acta 71 (2008) 688–6941.
[34] A. Ramoji, J. Yenagi, J. Tonannavar, V.B. Jadhav, M.V. Kulkarni, Spectrochim. Acta 68 (2007) 504–509.
[35] K.T. Vasudevan, M.V. Puttaraja, M.V. Kulkarni, Acta Crystallogr. C 47 (1991) 775–777.
[36] H.A. Sparkes, J.A.K. Howard, Acta Crystallogr. E 63 (2007) 3895.
[37] M.J. Frisch, G.W. Trucks, H.B. Schlegel, G.E. Scuseria, M.A. Robb, J.R. Cheeseman, J.A. Montgomery Jr., T. Vreven, K.N. Kudin, J.C. Burant, J.M. Millam, S.S. Iyengar, J. Tomasi, V. Barone, B. Mennucci, M. Cossi, G. Scalmani, N. Rega, G.A. Petersson, H. Nakatsuji, M. Hada, M. Ehara, K. Toyota, R. Fukuda, J. Hasegawa, M. Ishida, T. Nakajima, Y. Honda, O. Kitao, H. Nakai, M. Klene, X. Li, J.E. Knox, H.P. Hratchian, J.B. Cross, C. Adamo, J. Jaramillo, R. Gomperts, R.E. Stratmann, O. Yazyev, A.J. Austin, R. Cammi, C. Pomelli, J.W. Ochterski, P.Y. Ayala, K. Morokuma, G.A. Voth, P. Salvador, J.J. Dannenberg, V.G. Zakrzewski, S. Dapprich, A.D. Daniels, M.C. Strain, O. Farkas, D.K. Malick, A.D. Rabuck, K. Raghavachari, J.B. Foresman, J.V. Ortiz, Q. Cui, A.G. Baboul, S. Clifford, J. Cioslowski, B.B. Stefanov, G. Liu, A. Liashenko, P. Piskorz, I. Komaromi, R.L. Martin, D.J. Fox, T. Keith, M.A. Al-Laham, C.Y. Peng, A. Nanayakkara, M. Challacombe, P.M.W. Gill, B. Johnson, W. Chen, M.W. Wong, C. Gonzalez, J.A. Pople, Gaussian 03, Revision C.02, Gaussian, Inc., Wallingford, CT, 2004.
[38] G. Rauhut, P. Pulay, J. Phys. Chem. 99 (1995) 3093.
[39] Listing of vibrational scaling factors http://srdata.nist.gov/cccbdb/vibscalejust.asp.
[40] H.W. Thomson, P. Torkington, J. Chem. Soc. 171 (1945) 640.
[41] E.D. Glendening, J.K. Badenhoop, A.E. Reed, J.E. Carpenter, J.A. Bohmann, C.M. Morales, F. Weinhold, NBO 5.0, Theoretical Chemistry Institute, University of Wisconsin, Madison, 2001.
[42] G. Keresztury, S. Holly, J. Varga, G. Besenyei, A.Y. Wang, J.R. Durig, Spectrochim. Acta A 49 (1993) 2007.
[43] G. Keresztury, Raman spectroscopy theory, in: J.M. Chalmers, R. Griffith (Eds.), Handbook of Vibrational Spectroscopy, vol. 1, John Wiley & Sons, New York, 2002.
[44] Y. Erdogdu, O. Unsalan, M. Amalanathan, I. Hubert Joe, J. Mol. Struct. 980 (2010) 24–30.
[45] Y. Erdogdu, O. Ünsalan, D. Sajan, M.T. Güllüoğlu, Spectrochim. Acta A 76 (2010) 130–136.
[46] Y. Erdogdu, O. Ünsalan, M.T. Güllüoğlu, Turk. J. Phys. 33 (2009) 249–259.
[47] N.B. Colthup, L.H. Daly, S.E. Wiberley, Introduction to Infrared and Raman Spectroscopy, Academic Press, New York, 1990.
[48] B.C. Smith, Infrared Spectral Interpretation: A Systematic Approach, CRC Press, Boca Raton, FL, 1998.
[49] G. Socrates, Infrared and Raman Characteristic Group Frequencies – Tables and Charts, 3rd ed., J. Wiley & Sons, Chichester, 2001.
[50] K. Bahgat, Central Eur. J. Chem. 4 (4) (2006) 7735.
[51] L.J. Bellamy, the Infrared Spectra of Complex Molecules, Chapman and Hall, London, 1975.
[52] M. Gussoni, C. Castiglioni, J. Mol. Struct. 521 (2000) 1.
[53] D. Sajan, J. Binoy, I.H. Joe, V.S. Jayakumar, J. Zaleski, J. Raman Spectrosc. 36 (2005) 221.
[54] D. Sajan, I.H. Joe, V.S. Jayakumar, J. Zaleski, J. Mol. Struct. 785 (2006) 43.
[55] P.S. Soon, W.H. Gordon, J. Phys. Chem. 74 (1970) 4234.